Electronic Supporting Information

Mechanically responsive luminescent films based on copper iodide clusters

*Raquel Utrera-Melero,[a] Brendan Huitorel,[b] Marie Cordier,[c] Florian Massuyeau,[a] Jean-Yves Mevellec,[a] Nicolas Stephant,[a] Philippe Deniard,[a] Camille Latouche,[a] Charlotte Martineau-Corcos,[d,e] and Sandrine Perruchas[a,b]**

[a] Université de Nantes, CNRS, Institut des Matériaux Jean Rouxel, IMN, F-44000 Nantes, France.
Present address for S. Perruchas: Phone: (+33) (0)2 40 37 63 35. E-mail: sandrine.perruchas@cnrs-imn.fr
[b] Laboratoire de Physique de la Matière Condensée (PMC), CNRS - Ecole Polytechnique, 91128 Palaiseau Cedex, France.
[c] Université de Rennes, CNRS, ISCR (Institut des Sciences Chimiques de Rennes), UMR 6226, F-35000 Rennes, France.
[d] MIM, Institut Lavoisier de Versailles (ILV), UMR CNRS 8180, Université de Versailles St-Quentin en Yvelines (UVSQ), 45, avenue des Etats-Unis, 78035 Versailles Cedex, France.
[e] CEMHTI-CNRS, UPR 3079, 1D avenue de la recherche scientifique, 45071 Orléans Cedex 2, France

Synthesis of $[Cu_4I_4(PPh_2i\text{-}Pr)_4]$ (1). Copper(I) iodide and diphenyl-isopropylphosphine were purchased from Aldrich and used as received. To a suspension of CuI (213 mg, 1.1 mmol) in acetonitrile (5 mL) was added an acetonitrile solution (5 mL) of $PPh_2(CH(CH_3)_2)$ (250 mg, 1.1 mmol). The solution was stirring for 30 min and the formed precipitate was filtrated and rinsed with acetonitrile. **1** was recovered as a white crystalline powder. Yield = 92 %. ***1g*** was obtained by manually grind **1** in an agate mortar for 10 min.
Anal. Calcd for $C_{60}H_{68}Cu_4I_4P_4$: C 43.03, H 4.09.
Found for **1**: C 42.84, H 4.05.
Found for ***1g***: C 42.77, H 4.04.

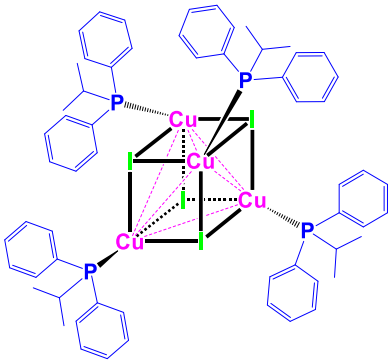

Figure S1. Schematic representation of the studied molecular copper iodide clusters formulated $[Cu_4I_4(PPh_2i\text{-}Pr)_4]$ (**1**).

Characterizations. Elemental analyses (C, H, N) were performed by the Service de microanalyses de l'ICSN - CNRS Gif-sur-Yvette. Thermogravimetric Analysis - Differential Scanning Calorimetry (TGA-DSC) analysis were performed with a NETZCH STA449 F3 equipment.

All solid-state NMR spectra were acquired on a Bruker Avance III 750 MHz NMR spectrometer (static magnetic field of B_0 = 17.6 T) using a 4 mm probe. The solid state static ^{63}Cu NMR spectra were recorded using the wideband uniform rate and smooth truncation (E. Kupce, R. Freeman, *J. Magn. Reson. Ser. A*, **1995**, *115*, 273.) Carr-Purcell Meiboom-Gill WURST-Q-CPMG (S. Meiboom, D. Gill *Rev. Sci. Instrum.*, **1958**, *29*, 688; H. Y. Carr, E. Purcell, *Phys. Rev.*, **1954**, *94*, 630; L. A. O'Dell, R. W. Schurko, *Chem. Phys. Lett.*, **2008**, *464*, 97.) pulse sequence, with an inter-pulse delay of 150 µs. The WURST pulse length was set 50 µs, with an excitation bandwidth of 1 MHz. 30 echoes were recorded. ^{1}H spinal64 (B. M. Fung, A. K. Khitrin, K. Ermolaev, *J. Magn. Reson.*, **2000**, *142*, 97.) decoupling was applied during signal acquisition. The recycle delay was set to 1 s. 384 and 2100 transients were acquired for **1** and **1*g***, respectively. The chemical shifts are externally referenced to CuI at 0 ppm. The ^{1}H-^{31}P cross-polarization (CP) magic-angle spinning (CPMAS) and ^{31}P-^{63}Cu *J*-based heteronuclear multiple-quantum coherence (*J*-HMQC) MAS NMR spectra were recorded at a MAS frequency of 12.5 kHz. The ^{1}H-^{31}P CP contact time was 3 ms. The recoupling time in the *J*-HMQC experiment was set to 320 µs (four rotor periods). ^{1}H-^{31}P CP was applied prior to the magnetization transfer for enhanced sensitivity. ^{1}H SPINAL-64 decoupling was applied during both excitation and reconversion periods and during the signal acquisition. A ^{63}Cu 90° pulse was applied after the reconversion period to remove antiphase coherence (C. Martineau, F. Fayon, C. Legein, J.-Y. Buzaré, G. Silly, D. Massiot, *Chem. Commun.* **2007**, 2720.). Recycle delay was 10 s. 32 transients were acquired for the CP MAS and 144 to 256 for the *J*-HMQC. The ^{31}P chemical shifts were referenced to a solution of H_3PO_4 at 0 ppm. The spectra were analyzed using the *dmfit* software (D. Massiot, F. Fayon, M. Capron, I. King, S. Le Calvé, B. Alonso, J.-O. Durand, B. Bujoli, Z. Gan, G. Hoatson, *Magn. Reson. Chem.* **2002**, *40* (1), 70).

Luminescence spectra were recorded with a Fluorolog 3 spectrofluorimeter (Horiba Jobin Yvon). Low temperature measurements were realized in an OptistatDN-V Oxford cryostat. The absolute internal quantum yields (Φ) were measured by using the Jobin Yvon integrating sphere. The error of the measured values has been evaluated to 10 %. Emission lifetimes (τ) were recorded with a time-resolved photoluminescence setup consisting of a frequency-tripled regenerative amplified femtosecond Ti:sapphire laser system from Spectra Physics to obtain λ_{ex} = 266 nm and a C7700 streak camera from Hamamatsu coupled to an SP2300 imaging Acton spectrograph for the luminescence detection. Data were analyzed by exponential curve fitting using *Origin* software.

Raman spectra in the 400-3500 cm^{-1} range were recorded with a Renishaw InVia Reflex spectrometer coupled with a Leica optical microscope. All spectra were recorded using an excitation wavelength of 633 nm emitted by a Helium Neon laser. Indeed, at this excitation energy, no photoluminescence hides the Raman effect. Rayleigh scattering was blocked by two successive edge filters, which allows the acquisition down to 100 cm^{-1}. The spectra from 45 to 400 cm^{-1} were measured with a Raman T64000 Jobin Yvon spectrometer (excitation wavelength 633 nm). In order to reach the lowest frequencies, the Rayleigh band was eliminated using a foremonochromator rather than edge filters.

Infrared (IR) spectra from 45 to 650 cm^{-1} were recorded with a Bruker Vertex 70 spectrometer using an adequate beamsplitter (polyethylene) and detector to reach far-IR frequencies. Samples were dispersed in pellets of polyethylene. From 400 to 4000 cm^{-1} the spectra were recorded with a Bruker Alpha Attenuated Total Reflectance (ATR) spectrometer.

Scanning Electron Microscopy (SEM) analysis of the films was performed with a field emission gun JEOL JSM 7600F at 5KV using a backscattered detector. EDX maps were performed at 10 KV with a BRUKER Silicone Drift Detector (SDD).

Single crystal X-Ray diffraction (SCXRD). Data were collected on a D8 Venture diffractometer equipped with a (CMOS) PHOTON 100 detector, using Mo-$K\alpha$ radiation (λ = 0.71073 Å, multilayer monochromator) at 150 and 293 K. The cell parameters were initially determined using more than 50 reflections. Experimental details are described in Table S1. The crystal structures were solved with SIR 97 and SHELXT-2014 and refined with SHELXL-2018/3 by full-matrix least-squares using anisotropic thermal displacement parameters for all non-hydrogen atoms. All the hydrogen atoms were placed in geometrically calculated positions. Details of the crystal data and structure refinements are summarized in Table S1.

Table S1. Crystal Data and Structure Refinement for **1** at 293 and 150 K.

	293 K	**150 K**
CCDC	2077585	2077584
T, *K*	293 K	150 K
Label	RUM-58-293	RUM-58-150
Chemical formula	$C_{60}H_{68}Cu_4I_4P_4$	$C_{60}H_{68}Cu_4I_4P_4$
fw	1674.78	1674.78
Crystal system	Monoclinic	Monoclinic
Space group	C2	C2
a, Å	19.9004(16)	19.7634(15)
b, Å	15.8409(12)	15.7529(12)
c, Å	14.0720(13)	13.9908(11)
α, deg	90.00	90.00
β, deg	134.996(2)	135.025(2)
γ, deg	90.00	90.00
V, Å^3	3137.0(5)	3078.6(4)
Z	2	2
ρ_{calc}, g/cm^3	1.773	1.807
μ, mm^{-1}	3.444	3.509
Reflections collected	35332	35334
Independent reflections	7247	7116
R_{int}	0.0450	0.0399
Reflections $I > 2\sigma(I)$	6637	6831
Parameters	330	330
GOF on F^2	1.080	1.104
$R_1{}^a/wR_2{}^b(I > 2\sigma(I))$	0.0321/0.0655	0.0244/0.0534
$R_1{}^a/wR_2{}^b(all)$	0.0391/0.0692	0.0268/0.0548

[a] $R_1 = [\Sigma\ abs(abs(F_O) - abs(Fc))]/ [\Sigma\ abs(F_O)]$. [b] $wR_2 = [\Sigma(w(F_O^2-F_c^2)^2)/ \Sigma[w(F_O^2)^2]^{0.5}$.

Table S2. Selected bonds lengths (Å) and angles (°) for **1** at 293 and 150 K.

	293 K	**150 K**
Cu-Cu	3.4112(15)*2 3.4115(19)*2 3.4392(12) 3.4383(25)	3.3821(9)*2 3.3824(14)*2 3.4030(16) 3.4066(12)
mean *Cu4(Å^3)*	*3,421(2)* *4,72(2)*	*3,390(1)* *4.59(1)*
Cu-I	2.6883(12)*2 2.7006(12)*2 2.7525(11)*2 2.6886(12)*2 2.6994(12)*2 2.7531(11)*2	2.6795(8)*2 2.6952(8)*2 2.7310(8)*2 2.6788(8)*2 2.6953(8)*2 2.7314(8)*2
mean *I4(Å^3)*	*2,7138(12)* *8.60(2)*	*2,7019(8)* *8.56(2)*
Cu-P	2.237(2)*2 2.238(2)*2	2.2333(15)*2 2.2354(15)*2
mean	*2,238(2)*	*2,2344(15)*
I-Cu-I	100.06(3)*2 100.09(3)*2 100.68(4)*4 101.43(4)*4	100.60(2)*2 100.61(2)*2 101.02(3)*2 101.14(3)*2 101.51(2)*2 101.56(2)*2
mean	*100,73(4)*	*101,07(3)*

Powder X-Ray diffraction (PXRD). Rietveld refinements were performed with the full-matrix least-squares technique using the Jana2006 program (V. Petricek, M. Dusek, L. Palatinus, **2006**) on powder patterns recorded at the Soleil synchrotron at Cristal beam line with the Dectris Mythen II detector (λ = 0.7289 Å). The cell parameters of **1** and **1*g*** were first refined but did not correspond to the SCXRD data indexed firstly in the tetragonal system. Indeed, a better fit was obtained with the I2 monoclinic space group which was then used to determine the crystalline structures. I2 space group has been chosen instead of the equivalent C2 one (SCXRD) to allow a better comparison with the genuine I-4 structure. The corresponding Rietveld pattern matchings are presented in Figure S5.

Table S3. Rietveld refinement data of **1** and **1*g***.

	Cell parameters	**Cu-Cu (Å)**	**Cu-I (Å)**
1	I2 a = 14.10126(13) b = 14.06951(11) c = 15.83035(8) Å γ = 90.0634(10) °	3.655(9) 3.397(9) 3.480(9) 3.397(9) *mean 3.482(9)*	2.634(10) 2.651(9) 2.673(8) 2.746(8) 2.835(8) 2.788(13) *2.72(1)*
1*g*	I2 a = 14.07839(16) b = 14.05648(16) c = 15.84125(11)Å γ = 90.0760(11) °	3.492(13) 3.420(10) 3.424(11) 3.342(12) *mean 3.420(13)*	2.800(13) 2.777(10) 2.680(10) 2.686(10) 2.612(15) 2.777(10) *2.72(1)*

All atomic positions (Cu, I, P, C) were refined excepted those of the hydrogen atoms. The ligands were refined considering a rigid-body mode. The determined structures of **1** and **1*g*** are shown in Figure S6 where all the atoms of **1*g*** are represented in green for clarity reason. Their superposition clearly shows their similarity and implies no strong structural modification. The Cu-Cu and Cu-I distances are reported in Table S3. The differences all lie within the experimental error value (error bars multiplied by the Berar's factor (J. F. Bérar, P. Lelann, *J. Appl. Crystallogr*. **1991**, *24*, 1)). The le Bail pattern matching were performed on laboratory data using the Jana2006 program too. The powder X-ray diffraction (PXRD) diagrams were recorded on a D8 Bruker diffractometer in the Bragg-Brentano geometry, equipped with a front germanium monochromator, a copper anode (CuK_α radiation ($\lambda = 0.1540598$ nm) and a LynxEye PSD detector. The calculated patterns were obtained from the single crystal data using the *Mercury* software.

Computational details. DFT computations were done using the B3PW91 functional associated to the LANL2DZ basis set augmented by polarization functions on all atoms. The Gaussian 16 suite of programs was used for all the calculations and post treatments were realized using the Gaussview, VMS and in-house python codes. All the geometries (ground and excited states) were relaxed and we took a particular care to check that these geometries were minima on their potential energy surfaces (PES). Atomic contribution on frontier orbitals were established thanks to the AOmix software. Absorption bands were assigned using the TD-DFT method on top of the ground state geometry. Vibrational contributions to electronic transition responsible for the observed luminescence were taken into account using the Vertical Hessian (VH) approach which takes into account mode-mixing between initial and final states. The lowest normal modes were neglected during the vibronic treatment in order to reach a sufficient progression (> 95 %).

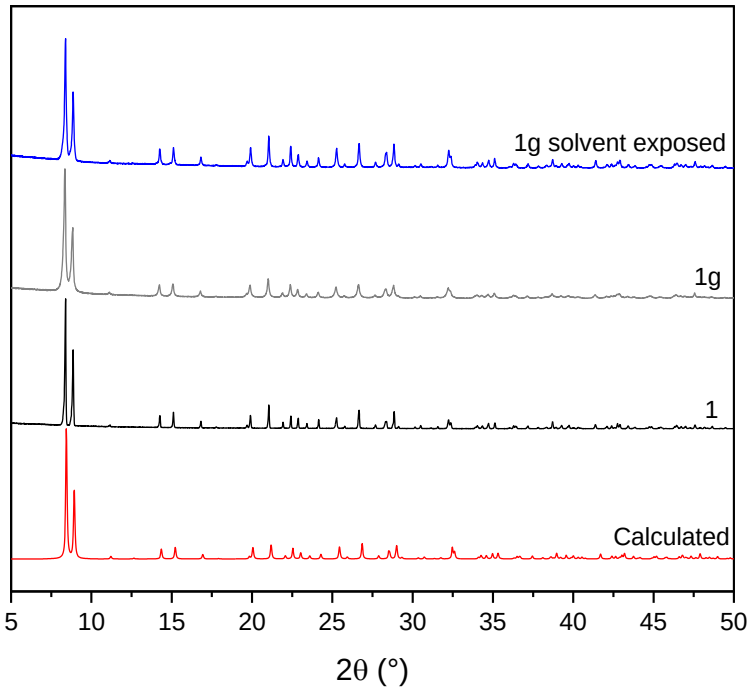

Figure S2. PXRD patterns of **1** and **1*g*** and after solvent exposure and calculated diagram from the SCXRD data.

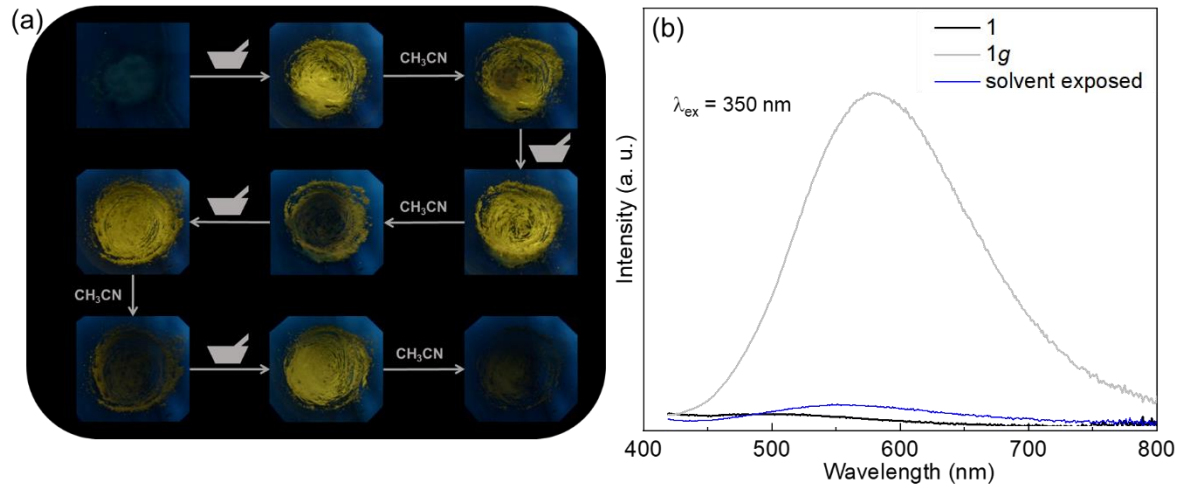

Figure S3. Reversibility of the luminescent mechanochromic properties of $[Cu_4I_4(PPh_2i\text{-}Pr)_4]$ (**1**). (a) Photos of powder of **1** after several cycles of manual grinding and acetonitrile exposure. (b) Emission spectra of **1** before and after grinding (**1g**) and after CH_3CN exposure.

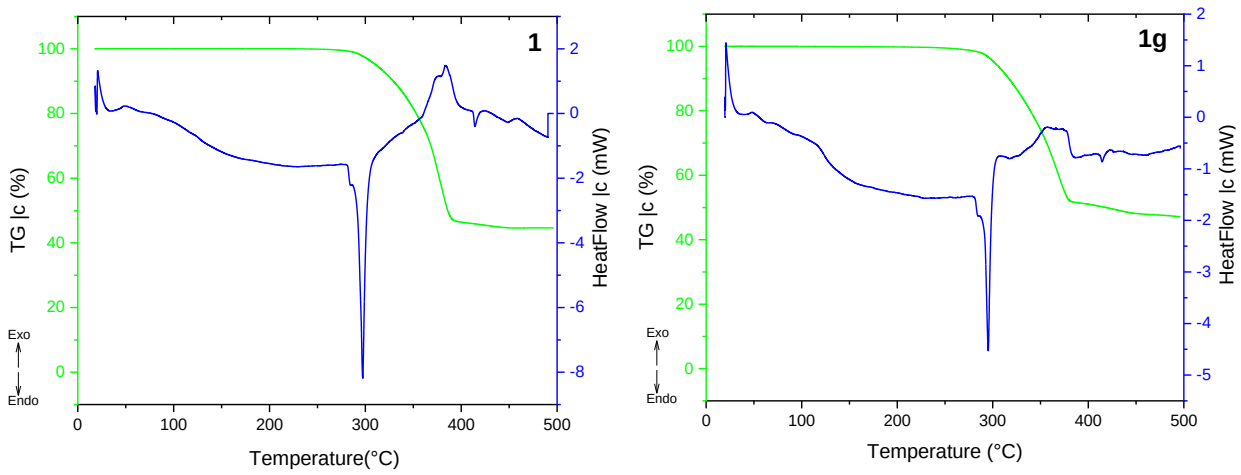

Figure S4.TGA/DSC curves of **1** and **1*g***.

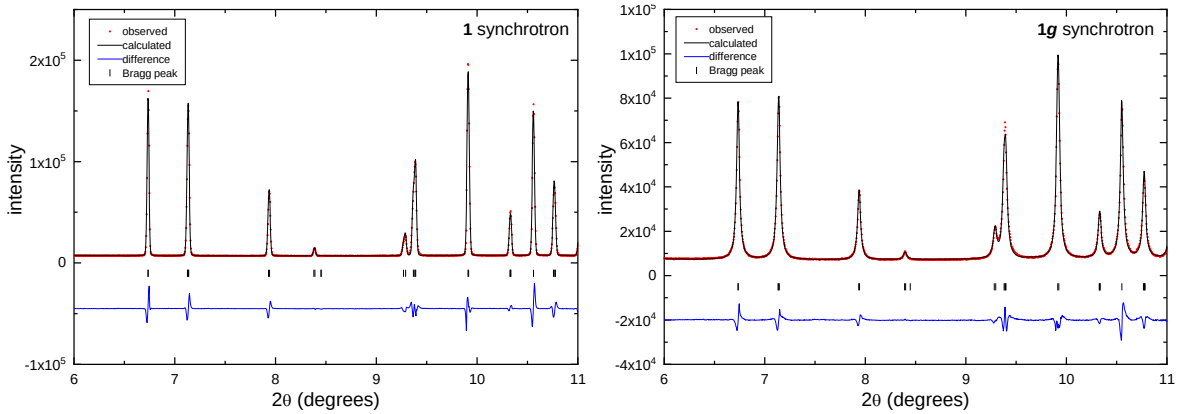

Figure S5. Synchrotron PXRD of **1** and **1*g*** and corresponding Rietveld pattern matching.

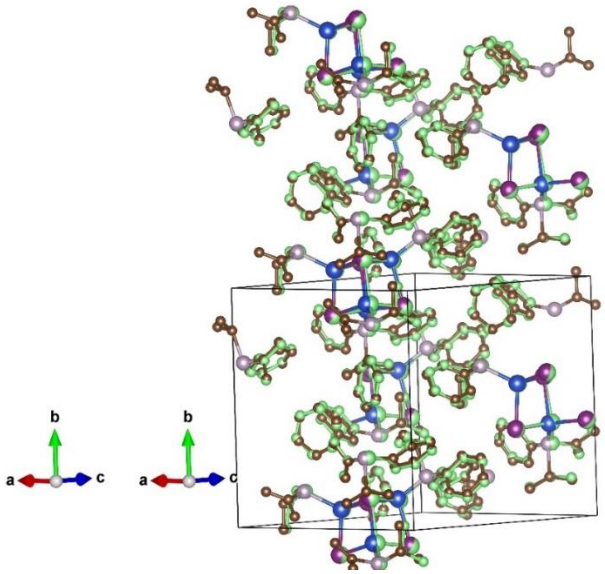

Figure S6. Superposition of the resolved crystalline structures of **1** and **1*g*** with Cu in blue, I in purple, P in grey and C in brown and all the atoms of the other structure are in green.

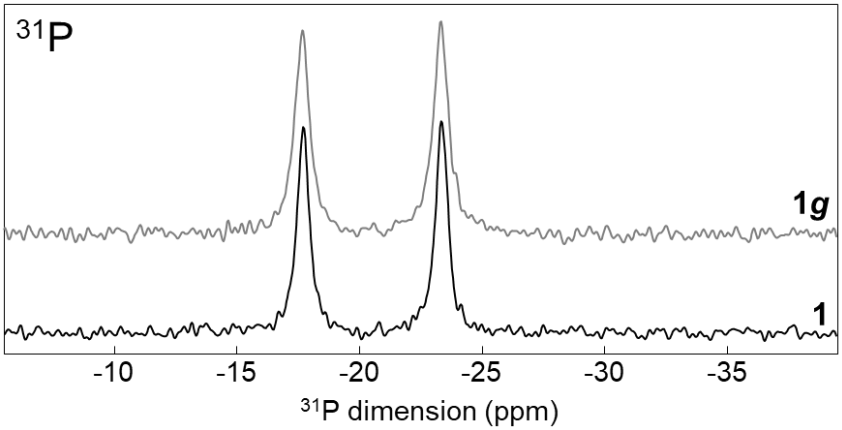

Figure S7. ^{31}P-^{63}Cu *J*-HMQC NMR spectra of **1** and **1*g***. The ^{31}P-^{63}Cu *J*-coupling value is 1707 Hz.

.

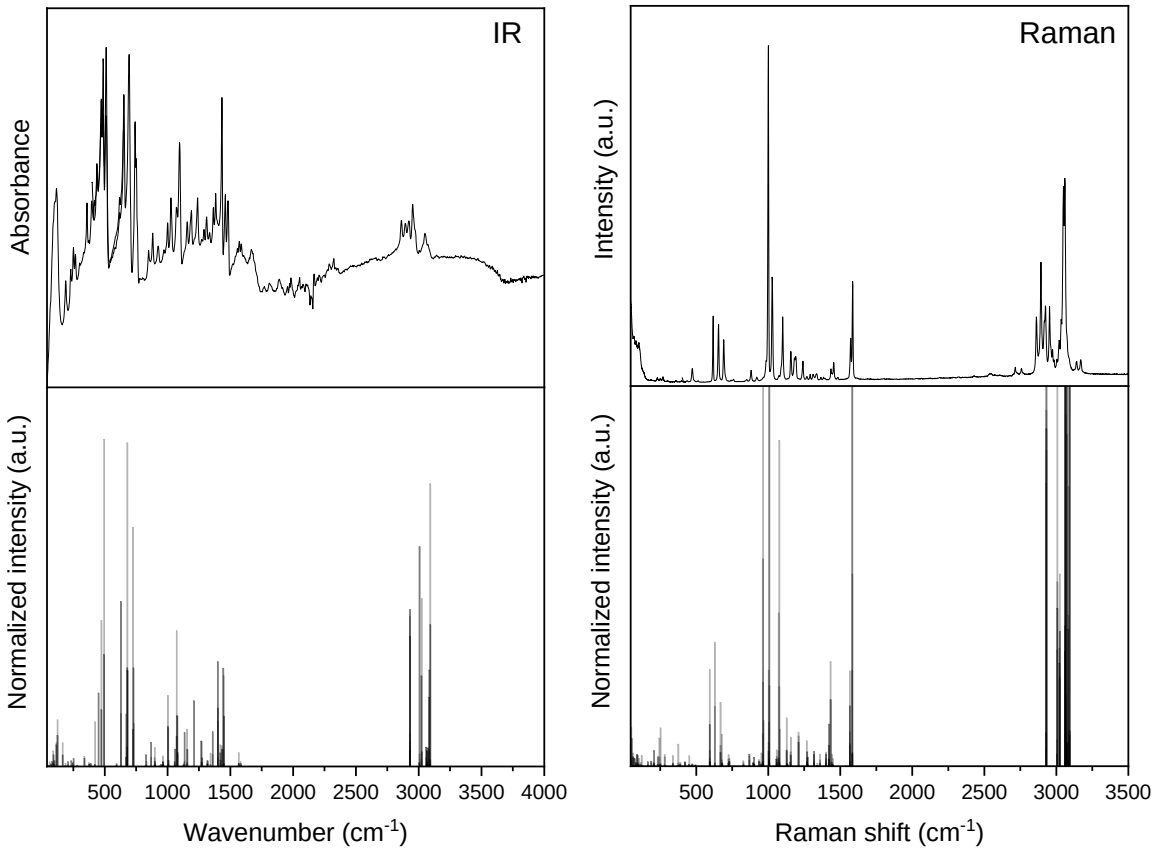

Figure S8. Experimental IR and Raman spectra (top) and DFT calculated IR intensities and Raman activities (bottom) of $[Cu_4I_4(PPh_2i\text{-}Pr)_4]$ (**1**).

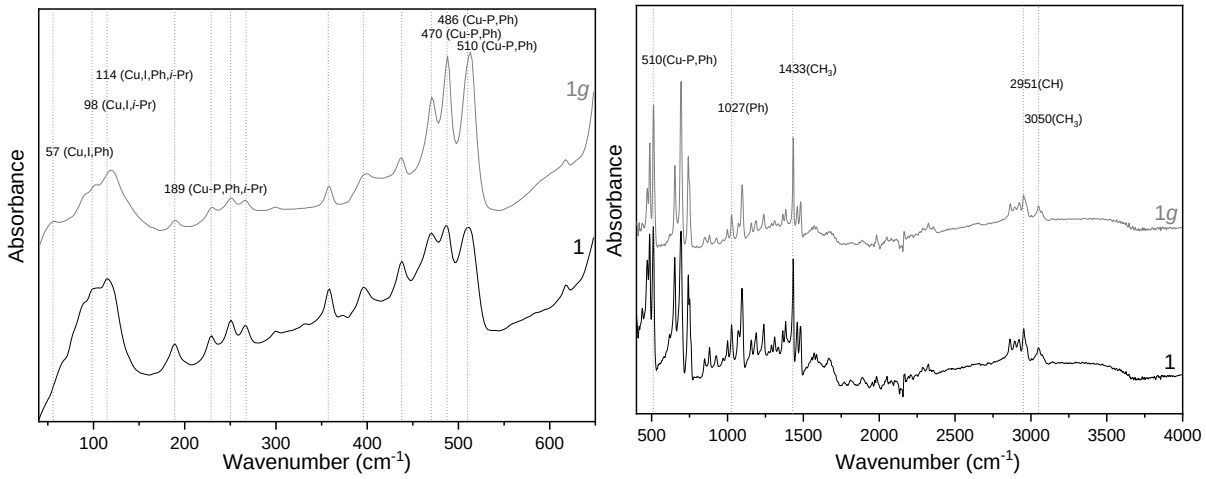

Figure S9. Experimental IR spectra of **1** and **1*g***.

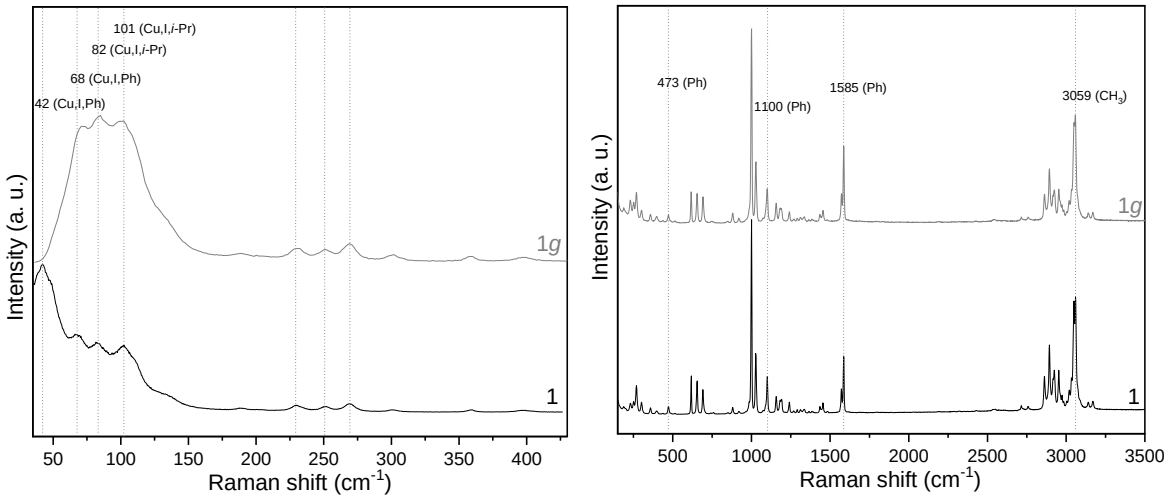

Figure S10. Experimental Raman spectra of **1** and **1*g***.

Table S4. Experimental and computed (after a scale factor 0.96, in square brackets) IR wavenumbers (cm^{-1}) of **1** and **1*g*** under 200 cm^{-1}.

1	**1*g***	**Assignment**
	57 [56]	Cu, I, and Ph (cluster core rocking/twisting)
98 [99]	102	Cu, I and *i*-Pr (Cu-Cu wagging)
114 [114, 116, 124]	119 (br)	Cu, I, Ph and *i*-Pr.(Cu_4 core wagging + Cu_4 core breathing + I_4 breathing and rocking)
189 [188]	189 (br)	Cu-P, Ph and *i*-Pr

Table S5. Experimental and computed (after a scale factor 0.96, in brackets) Raman shifts (cm^{-1}) of **1** and **1*g*** under 200 cm^{-1}.

1	**1*g***	**Assignment**
42 [42]		Cu, I, and Ph (cluster core rocking/twisting). Ph rocking
68 [66]	72	Cu, I and Ph (Cu-I twisting)
82 [90]	85	Cu, I and *i*-Pr (Cu-Cu wagging)
101 [103]	101	Cu, I and *i*-Pr (Cu-Cu torsion)

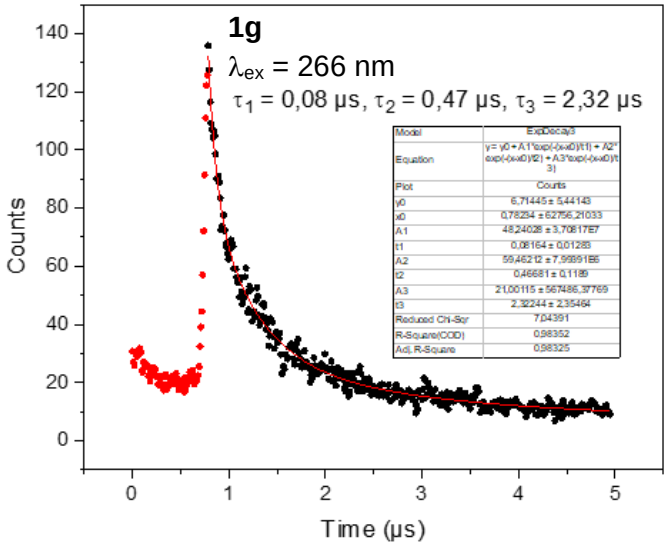

Figure S11. Fitted emission decay curve of **1*g***.

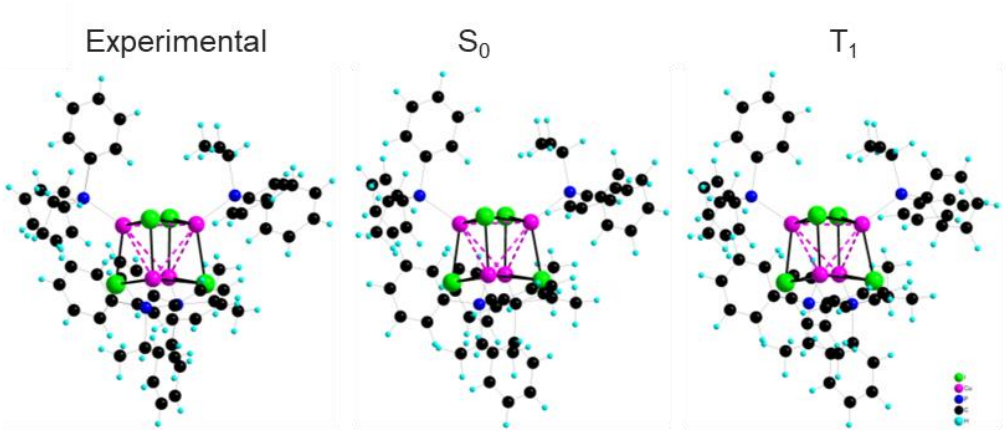

Figure S12. DFT optimized molecular structure of **1** at the fundamental (S_0) and the excited state (T_1) compared with the experimental SCXRD one.

Table S6. Averaged geometrical parameters of the optimized DFT structures of **1** at the S_0 and T_1 states along with the SCXRD data at 150 K reported in square brackets.

	[$Cu_4I_4(PPh_2i\text{-}Pr)_4$] (1)	
	S_0	**T_1**
HOMO-LUMO gap (eV)	4.15	-
Cu-Cu (Å)	3.381 [3.390(1)]	3.343
Cu-I (Å)	2.744 [2.702(1)]	2.737
Cu-P (Å)	2.328 [2.234(1)]	2.335

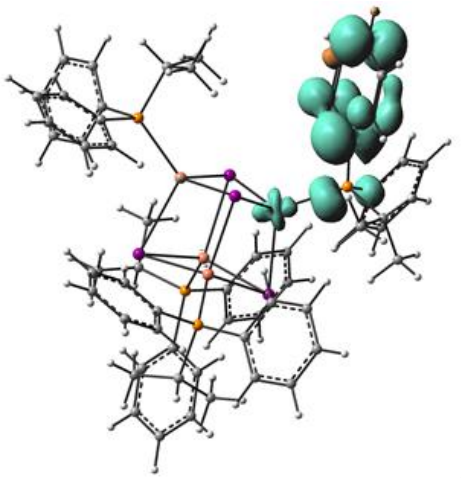

Figure S13. Spin density calculated for the triplet state (T_1) of **1**.

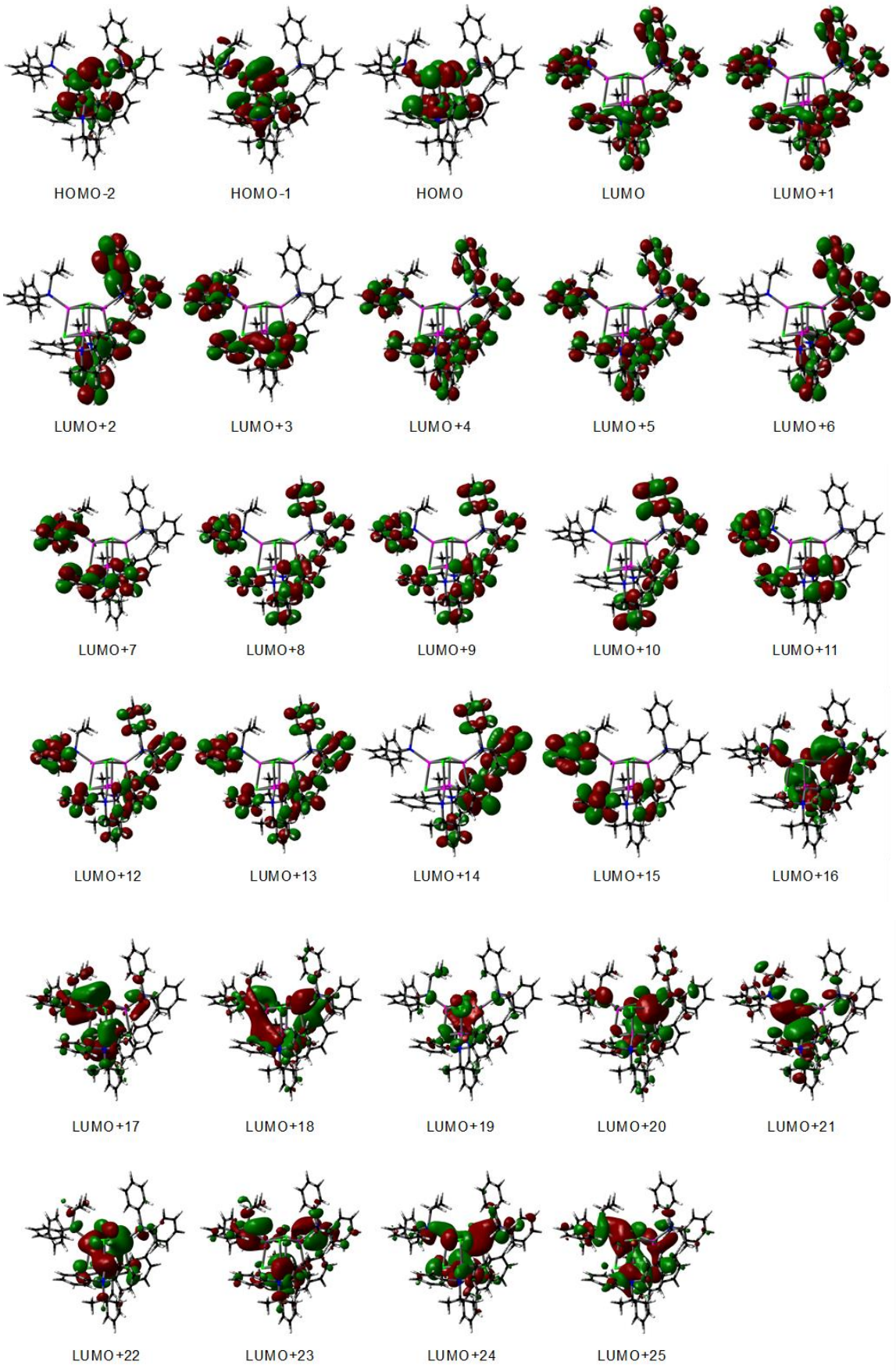

Figure S14. Calculated molecular orbitals of **1** at S_0.

Table S7. Calculated and experimental optical data for **1**. Values in parenthesis are the oscillator strengths (> 0.01) associated with the absorption wavelengths. Only the major contributions to these transitions are indicated with their corresponding percentage.

	[$Cu_4I_4(PPh_2$*i*-Pr$)_4$] (1)	
	Experimental	**Calc. wavelength (oscillator strength) assignment [symetry]**
Absorption λ (nm)	**330** (broad)	**344** (0.016) *Cu/I* → π^* *phenyl* [E] HOMO-2 → LUMO (40%), HOMO-2 → LUMO+1 (31 %), HOMO → LUMO+2 (25 %) **343** (0.017) *Cu/I* → π^* *phenyl* [B] HOMO-2 → LUMO+2 (29 %), HOMO-1 → LUMO+3 (29 %), HOMO → LUMO+1 (40 %) **321** (0.039) *Cu/I* → π^* *phenyl* [E] HOMO-2 → LUMO+4 (46 %), HOMO-2 → LUMO+5 (32 %), HOMO → LUMO+6 (17 %) **320** (0.031) *Cu/I* → π^* *phenyl* [B] HOMO-2 → LUMO+6 (19 %), HOMO-1 → LUMO+7 (19 %), HOMO → LUMO+4 (58 %)

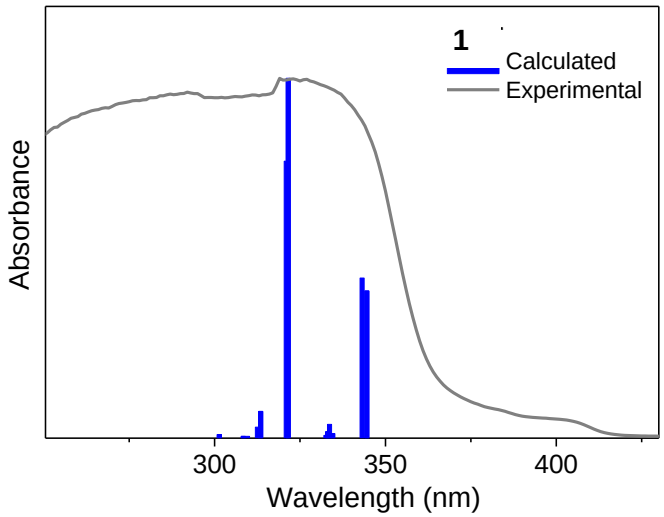

Figure S15. Calculated oscillator strengths and experimental diffuse reflectance spectra of **1**.

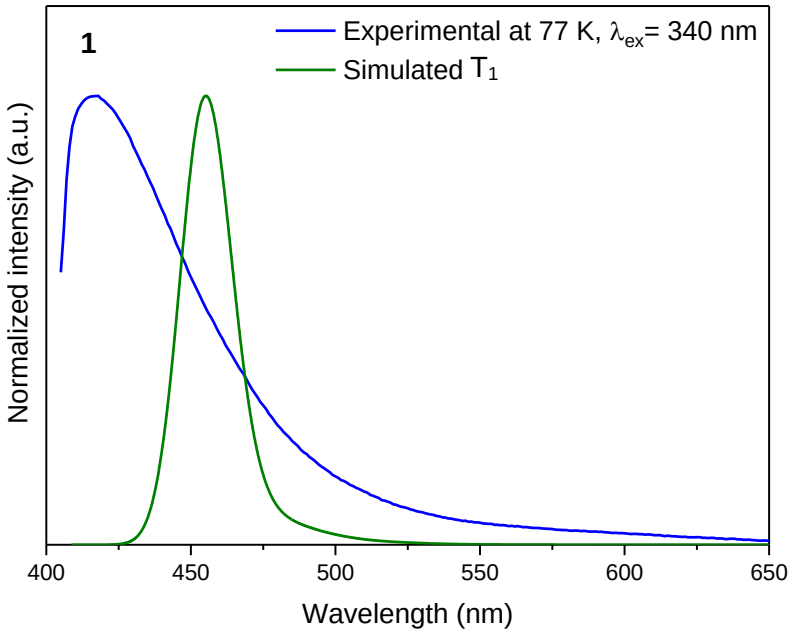

Figure S16. Simulated and experimental emission spectra of **1**.

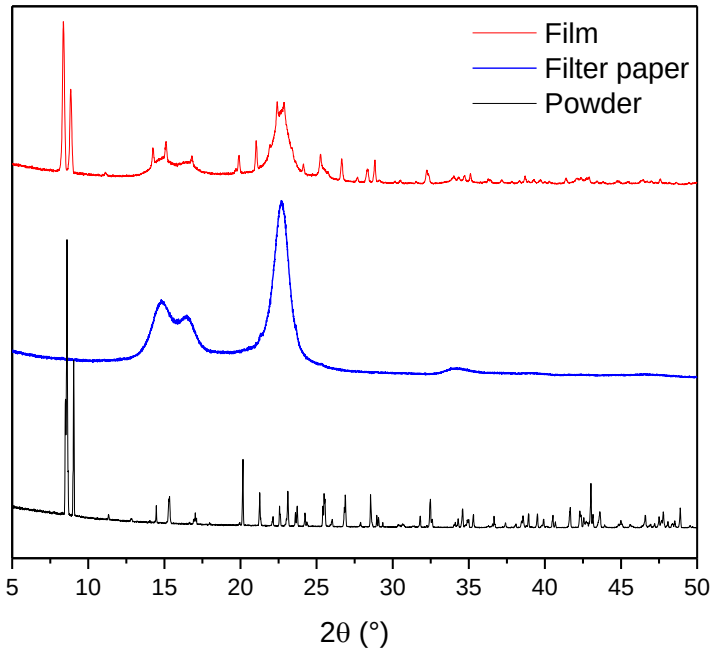

Figure S17. PXRD patterns of mechanochromic films of **1**.

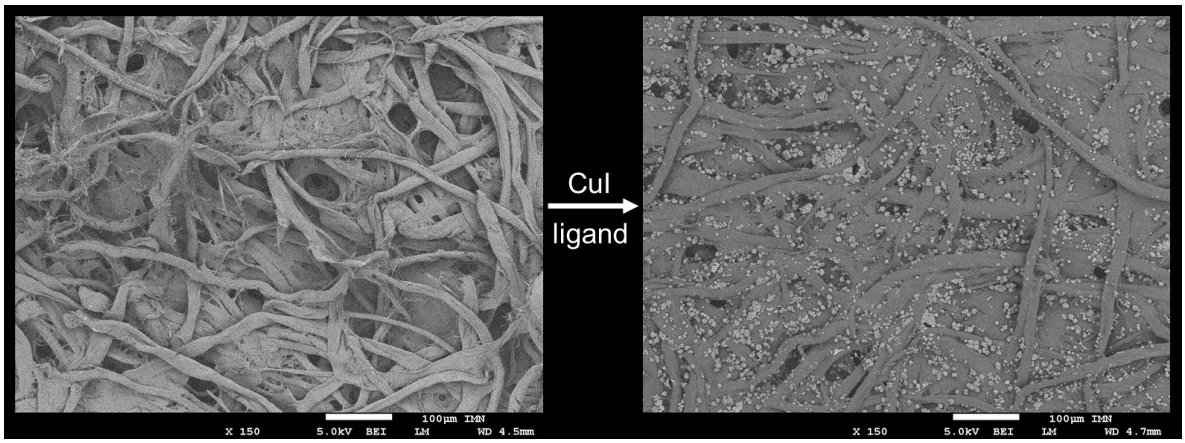

Figure S18. SEM images of the paper used as substrate for the luminescent mechanochromic films, before and after *in-situ* synthesis of **1**.

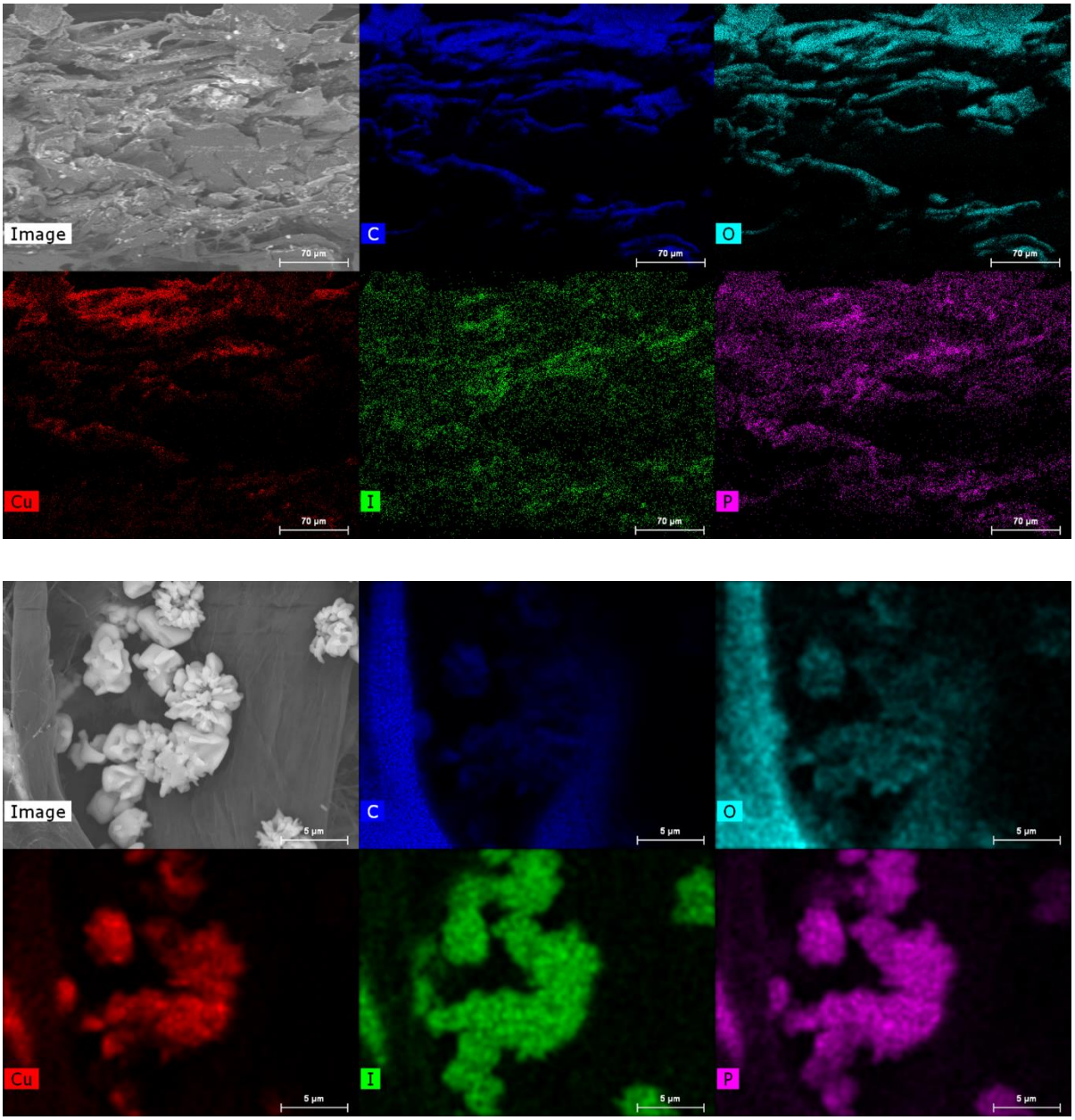

Figure S19. SEM-EDX analyses of the mechanochromic film of **1** in cross-section (top) and at the surface (bottom). The black areas (top images) are due to shadows of the surface's topography.